Microsyst Technol (2010) 16:1485–1493
DOI 10.1007/s00542-010-1020-1

TECHNICAL PAPER

Manufacture of microfluidic glass chips by deep plasma etching, femtosecond laser ablation, and anodic bonding

S. Queste · R. Salut · S. Clatot · J.-Y. Rauch · Chantal G. Khan Malek

Received: 31 July 2009 / Accepted: 5 January 2010 / Published online: 26 January 2010

Abstract Two dry subtractive techniques for the fabrication of microchannels in borosilicate glass were investigated, plasma etching and laser ablation. Inductively coupled plasma reactive ion etching was carried out in a fluorine plasma (C_4F_8/O_2) using an electroplated Ni mask. Depth up to 100 μm with a profile angle of 83°–88° and a smooth bottom of the etched structure (Ra below 3 nm) were achieved at an etch rate of 0.9 μm/min. An ultrashort pulse Ti:sapphire laser operating at the wavelength of 800 nm and 5 kHz repetition rate was used for micromachining. Channels of 100 μm width and 140 μm height with a profile angle of 80–85° were obtained in 3 min using an average power of 160 mW and a pulse duration of 120 fs. A novel process for glass–glass anodic bonding using a conductive interlayer of Si/Al/Si has been developed to seal microfluidic components with good optical transparency using a relatively low temperature (350°C).

1 Introduction

Glass has many useful properties that make it an important material for microsystem technology, in particular for optofluidic-based applications. Due to its excellent optical transmission it enables visual inspection and optical detection within the microfluidic channel or reactor. Its good chemical resistance as well as its high thermal stability make it compatible with numerous operating conditions and applications. Other beneficial properties of glass are chemical inertness, electric insulation as well as its hardness and good mechanical stability. It also has established schemes for surface modification and functionalisation.

Challenges concerning the manufacture of microfluidic devices in glass include making precise anisotropic structures with high aspect ratio at the micro and nanoscale as well as hermetic sealing with a transparent cover plate. In this work, two different dry subtractive techniques were employed to structure glass for microfluidic applications, plasma-based reactive ion etching (RIE) using an inductively-coupled-plasma (ICP) RIE system and femtosecond laser ablation. Concerning the sealing of a glass substrate, a process using anodic bonding with an intermediate conductive layer was developed.

2 Techniques employed for micromachining the microfluidic circuit in glass

2.1 Deep plasma etching

Plasma-based RIE is a very controllable dry process exploiting both chemical and physical processes to remove solid material locally. It is used for anisotropic and precise micro-scale etching of materials. In particular, ICP-RIE has demonstrated its potential in batch fabrication of high speed directional deep etching of microstructures in silicon with high aspect ratio, which produced great impact on MEMS device fabrication. More recently, high speed directional etching using ICP plasma has being extended to materials other than silicon. However, in contrast to the well-established deep silicon etching, the plasma etching of non conventional materials such as glass has suffered from limitations related to the chemical composition of materials

S. Queste · R. Salut · S. Clatot · J.-Y. Rauch · C. G. Khan Malek (✉)
FEMTO-ST Institute, CNRS UMR 6174,
32 Avenue de l'Observatoire, 25044 Besançon, France
e-mail: chantal.khanmalek@femto-st.fr

and the formation of non-volatile compounds during plasma etching.

Plasma etching of various types of silica-based oxide glass materials (soda-lime glass, borosilicate glass, fused silica a.k.a. amorphous "quartz", etc.) has been reported by several authors (Li et al. 2001, 2002; Ichiki et al. 2003; Ceriotti et al. 2003; Park et al. 2005; Jung et al. 2006; Akashi and Yoshimura 2006; Baram and Naftali 2006; Goyal et al. 2006; Thiénot et al. 2006; Kolari et al. 2008; Kolari 2008a, b) using various fluorine- and fluorocarbon-based chemistries (C_4F_8, CHF_3, CF_4, SF_6). However, they are characterized by low etch rates, a low selectivity to etch mask, and rough surfaces, which limit the formation of deep and high-aspect-ratio microstructures, even using high density plasma sources such as in ICP-RIE etchers.

2.2 Femtosecond laser ablation

Lasers provide a flexible and versatile technology platform for creating micro and nanostructures in a variety of materials. Laser micromachining is a direct write and etch technique, therefore does not require any mask or post-development steps. It is a suitable technique for rapid prototyping of microsystems, and in particular microfluidic devices. Several groups have also investigated the use of various lasers and processes to machine glass substrates. One of the issues is the brittleness and poor thermal properties of most glasses, making the fabrication of finely machined features a difficult task.

Recent developments in high-power ultra-short pulse laser technology have opened up completely new possibilities for precise and fine processing in almost any kind of materials, both absorptive and transparent ones. In particular, a unique feature of laser micromachining using femtosecond lasers is that it makes possible precise delivery of high density energy in a highly controlled and spatially localized way. The non linear absorption induced by the very extremely high peak intensity in the pulse focus ensures that the absorption, and therefore material removal, is confined to the vicinity of the focus, leaving the rest of the substrate unaffected, thus allowing ultra-precision micro-machining.

Interest for femtosecond laser micromachining of glass substrates for microfluidic applications is growing. Some groups use a combination of femtosecond exposure to modify the glass material and wet-etching (Marcinkevičius et al. 2001; Bellouard et al. 2004; Cheng et al. 2004; Maselli et al. 2007; Sato et al. 2007; An et al. 2008) while others produce directly microstructures by laser ablation in glass (Shah et al. 2001; Giridhar et al. 2004; Karnakis et al. 2005; Nikumb et al. 2005; An et al. 2006; Schafer et al. 2009).

3 Experimental and results

3.1 Samples

The work was performed using 3″ double-side polished borosilicate glass wafers composed of silicon oxide (81%) and boric acid (B_2O_3 13%) as their main component (Borofloat® 33 and Pyrex® 7740 differ as regards their chemical composition in the alkali ratio of Na_2O to K_2O and in their content of so-called oxidic minor components and impurities—Pyrex® 7740 is known to have a typical composition of SiO_2 (80.6%), B_2O_3 (13.0%), NaO_2 (4%), Al_2O_3 (2.3%), and K_2O_3 (0.04%), whereas that of Borofloat® 33 is 81% SiO_2, 13% B_2O_3, 4% Na_2O/K_2O, and 2% Al_2O_3).

Glass wafers of 500 μm thick Borofloat® 33 (Schott) and Pyrex® 7740 (Corning) were used respectively for plasma etching and femtosecond laser machining, and 1 mm thick Borofloat®33 (Schott) as cover wafer for anodic bonding.

For the electroplated mask used for ICP-RIE, an 8 μm thick layer was electroplated in an AZ9260 (AZ-Electronic Materials®)) photoresist stencil defined by photolithography on the glass substrate coated with an adhesion layer of chromium (20 nm) and seed layer of copper (200 nm). A typical Watts bath based on Ni sulfamate (lower stress than Ni sulfate) at a current density of 1.5 A/dm^2 and a bath temperature of 50°C was used for Ni electroplating. At the end of the process the photoresist was removed by acetone and the Cr/Cu plating layer by RIE.

3.2 Deep plasma etching

The etching is carried out using a multiplex AOE reactor of STS with an ICP RF generator of 3 kW and a RIE generator of 1.5 kW. The maximum size of the wafer is 6 in., and the gases available are SF_6, CF_4, C_4F_8, He, O_2 and Ar. The temperature of the substrate holder was varied between 20 and 80°C. The gas mixture used for glass etch was C_4F_8/O_2. The samples were contacted to Si carriers with thermal grease for cooling. Step heights were obtained with a Tencor Alpha-step profilometer. Selectivity and etch rate were estimated from scanning electron microscope (SEM) images normalized against profile measurements of the same feature. A profile angle, α, was calculated geometrically from the difference between the top and bottom widths over the etch depth, for narrow trenches and also large open features. This angle reflects the verticality of the wall, with α equal to 90° for a perfectly vertical wall.

Best results were obtained using a pressure of C_4F_8/O_2 plasma of 8 mTorr with a bias power of 600 W and an 8 μm thick electrodeposited Ni etch mask. A depth of up to 120 μm with an aspect ratio of 20 was achieved with an

etch rate comprised between 0.7 and 1 μm/min depending on the size of the structures, an etch selectivity of 18:1, and angles of 83°–88°. The bottom of the etched structures was smooth (Ra 10–30 nm), indicating a very limited surface degradation during the process. Figures 1 and 2 show examples of such etching.

These results are competitive with those found in the literature. The aspect ratio of 40:1 which is obtained here is the best obtained for glass etching with ICP-RIE technique when compared to others significant studies such as 10:1 as obtained by Kolari et al. (2008) on sub-micrometer wide structures using an AlN etch mask and SF_6 chemistry in fused silica (Kolari et al. 2008), and 10 for a trench pattern etched in SF_6 (Li et al. 2002).

Concerning deep etching of glass using ICP-RIE etcher, Li et al. (2001, 2002) first presented ICP-RIE of borosilicate glass using a Ni electroplated mask in SF_6 plasma. They achieved one of the best results today with a depth of 200 μm (through-wafer etching) with a taper of 88°, as well as a high etch rate (0.6 μm/min) and a smooth surface Ra of ~4 nm. Park et al. (2005) also etched borosilicate glass using an electroplated Ni etch mask in SF_6 with an etch rate of 0.75 μm/min but observed undercut in the etch mask and microtrenching at the bottom of the trench, due to redeposition of non-volatile products. Shifting to a more physical etching process with an SF_6/Ar plasma corrected this effect and led to more vertical etch profile angle (88°) but resulted in a decreased etch rate (0.54 μm/min). The highest etching speed was obtained by Ichiki et al. (2003) with 1.2 μm/min using a SF_6 plasma chemistry. Akashi and Yoshimura (2006) used a 200 μm silicon-bonded wafer as etch mask and demonstrated the etching of 430 μm deep groove of 1 mm size with 80° in a C_4F_8 plasma. Kolari also used a C_4F_8-based plasma chemistry and a silicon DRIE-etched shadow etch mask clamped on the glass wafer to produce a 250 μm deep nozzle with an angle of 80°–86° (Kolari 2008a, b) and over 300 μm deep structures in Pyrex and silica with aspect ratio over 3 using a C_4F_8/He/O_2 plasma chemistry (Kolari et al. 2008). They showed that a full thickness silicon wafer (400 μm) is not appropriate for feature sizes below 200 μm width.

For etch depth of 100 μm, Kolari et al. (2008) also used amorphous silicon, electroplated Ni, and thick SU-8 layers which all gave reasonable wall verticality (80°–86°) and an aspect ratio of 3 in the deep etching of Pyrex and fused silica. We obtained a maximum depth of 120 μm with an aspect ratio of 6 using an electroplated Ni mask (Queste et al. 2008). This result is comparable with the results of Li et al. (2001) and Kolari et al. (2008).

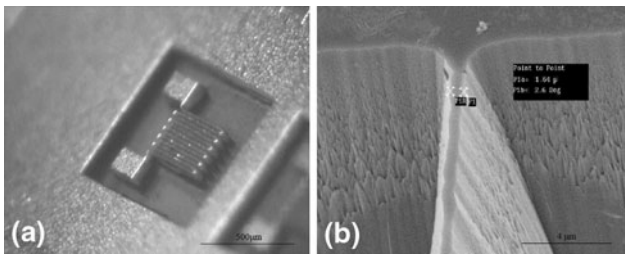

Fig. 2 Glass ICP-etched microstructure with an etch depth of 80 μm and sidewalls verticality of 85°: **a** optical image of the overall structure; **b** SEM image of detail showing a wall of 2 μm width and 80 μm height (aspect ratio 40)

We report a relatively high etch rate of 1 μm/min which is better than most results obtained with the C_4F_8, SF_6, and C_4F_8/O_2 which range from 0.5 to 0.75 μm/min.

Qualitatively the sidewalls exhibit some roughness as can be seen on the SEM picture of the Fig. 3a. However, the bottom of the etched structures is smooth and has an arithmetic roughness (Ra) of 30 nm, as measured with a Tensor Alpha-step IQ profilometer (Fig. 3b). This roughness is larger at the top of the sidewall as compared with the bottom of the etched structure. This roughness difference is attributed to the damage caused to the electroplated Ni mask by the ion bombardment during etching.

Concerning the etch profiles, the angles of 82°–88° using a C_4F_8/O_2 plasma are on the same order of magnitude as that reported by Ichiki et al. (2003), 89°, using an SF_6/Ar plasma chemistry or the 79°–88° of Li et al. (2001) with SF_6 or 80°–86° of Kolari (2008a, b) using C_4F_8 plasma. There is very little information about bottom roughness of etched structures; we report a roughness of 2 nm (Ra) for shallow etching below 20 μm, this value being comparable to the 1.97 nm presented by Goyal et al. (2006) for 20 μm etch depth but with a different etching chemistry C_4F_8/O_2 instead of SF_6/Ar. This value increases to 10 nm for an etching depth of 120 μm.

Table 1 summarizes the major parameters and results obtained by the various authors and discussed above.

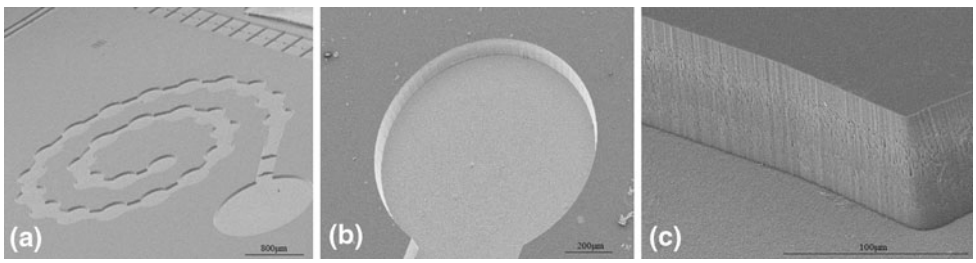

Fig. 1 DRIE etched microfluidic circuit in borosilicate glass: **a** 70 μm deep microfluidic circuit; **b** close-up view of the reservoir; **c** detail of the wall of the channel

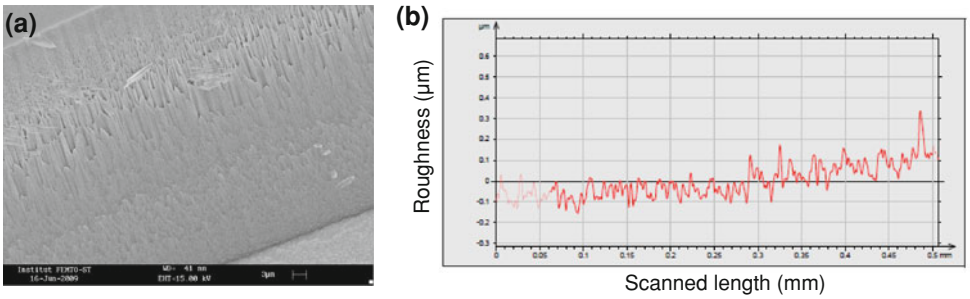

Fig. 3 **a** SEM of sidewalls exhibiting some roughness; **b** roughness profile of the bottom of etched structures as a function of scanned length

Table 1 Major parameters and results in DRIE etching of glass from our work and from the literature

Reference	Mask type	Etching chemistry	Etching depth (µm)	Etching rate (µm/min)	Profile	Roughness Ra (nm)	Aspect ratio
Our work	Ni 8 µm	C_4F_8/O_2	120	1	83°–88°	2–10	40
Akashi and Yoshimura (2006)	Si wafer 200 µm	C_4F_8	430		80°		
Goyal et al. (2006)	Ni 5 µm	SF_6/Ar	20	0.536		1.97	
Ichiki et al. (2003)	Cr	SF_6	<20	1.2	88°	Very high	
Kolari et al. (2008)	Si wafer 400 µm	C_4F_8/He/O_2	250	0.5	80°–86°		<3
Kolari et al. (2008)	Si wafer 400 µm	C_4F_8/He/O_2	300	0.35			3
Kolari et al. (2008)	Ni 5 µm	C_4F_8/O_2	80	0.7	80°–86°		3.5
Li et al. (2001)	Ni	SF_6	200	0.6	88°	4	10
Park et al. (2005)	Ni	SF_6	40	0.75	<88°		
Park et al. (2005)	Ni	SF_6/Ar	27	0.54	88°		
Queste et al. (2008)	Ni 6 µm	C_4F_8/O_2	120	0.8	83°–88°	2	6

3.3 Femtosecond laser micromachining

The laser system comprises a mode-locked laser oscillator (Spectra Physics MaïTaï) coupled to a Ti:sapphire regenerative amplifier (Spectra Physics Spitfire), producing pulses of 100 fs duration at a wavelength of 800 nm. The repetition rate of the pulses is 5 kHz. The maximum output power of the laser is 2.2 W at 5 kHz, that is a maximum energy and output power of respectively 0.44 mJ and 4.4 GW per pulse of 100 fs.

Direct-write laser ablation was carried out in a micromachining station (Astree 250 from Novalase; http://www.novalase.com). The power of the laser beam is controlled by a motorized attenuator, which consists of a half-wave plate. The laser was focused to a 10 µm spot size using an objective lens of 50 mm focal length. After beam shaping, the repetition rate was 5 kHz, the pulse duration 120 fs, the average power comprised between 30 and 160 mW. Writing of the patterns can be performed by scanning of the laser beam on the sample placed in the focal plane with a field size of 2 cm × 2 cm and/or translation of the sample mounted on a computer-controlled 3D stage through the focal region of the laser beam (moving stage accuracy: 1 µm). The field size was large enough for the following experiment, so only the beam was scanned (stage still). All of these parameters are controlled by the software. The micromachining was performed at atmospheric pressure with a local aspiration.

The depth of the channel shows a linear dependence on the number of passes. The maximum aspect ratio that can be obtained with our present set-up is around 4–5 with minimum feature sizes of 15 µm. Channels of 100 µm width, 140 µm height and 4 mm length were written in 3 min using a spot size of 10 µm with an average power of 160 mW at 5 kHz, that is with a pulse energy of 0.0 32 mJ and a power of 0.27 GW (pulse duration of 120 fs). The etching speed is then 0.1 mm^3/mn. Figure 4 shows details of the microfluidic chip. The strategy is to write lines spaced by 5 µm along the largest dimension. The channel was written first, then the reservoir, which causes the pitting in the overlapping zone which can be seen in Fig. 4a. The profile angle is comprised between 80° and 85°. The surface is smooth around the machined areas. The bottom roughness is a bit high, on the order of 100–150 nm (Ra) (Fig. 4d).

Applications of femtosecond laser direct ablation are limited to micromachining processes where the total volume of ablated material is rather small. Strategies to increase the etching speed include increasing the pulse power but this approach is limited due to the limited average power output of ultra short pulse laser systems, including our femtosecond laser system for which it is not

possible at the moment to increase more the laser beam power to machine the glass faster. In the future, if we manage to improve the optical path, machining at higher speed may be possible but we do not know if the glass will resist, because it is very brittle. Cracks around the machined areas and/or break of the wafer could occur.

3.4 XPS measurements

XPS measurements were realized before and after etching on femtosecond laser ablated and ICP-etched glass surfaces (Fig. 5, 6 respectively).

The XPS analysis was carried out using an Alpha 110 Thermo VG Scientific apparatus composed of a 200 W Al source coupled with a 3 kV Argon ion gun at a pressure of 5×10^{-8} mbar during 60 s. In each case, three runs of analysis/etch steps were used in order to degas the surface, clean it from pollution, and find the composition of the bulk materials.

The widescan spectra corresponding to the virgin borofloat or Pyrex surface (Fig. 5α) exhibited peaks which are attributed to oxygen (O1s, 531 eV), carbon (C1s, 285 eV), aluminum (Al2s, 120.5 eV; Al2p, 75.7 eV) and silicon (Si2s, 153 eV; Si2p, 99.8 eV). After three etching runs using the ion gun of the XPS analyzer (Fig. 5γ), the carbon species present at the surface (carbon surface contamination giving the C1s peak at 285 eV) was decreased. In the case of the glass surface ablated by femtosecond laser, the XPS spectrum did not indicate any change in the composition of the surface, except for the carbon peak which showed a similar trend as described above (Fig 5β).

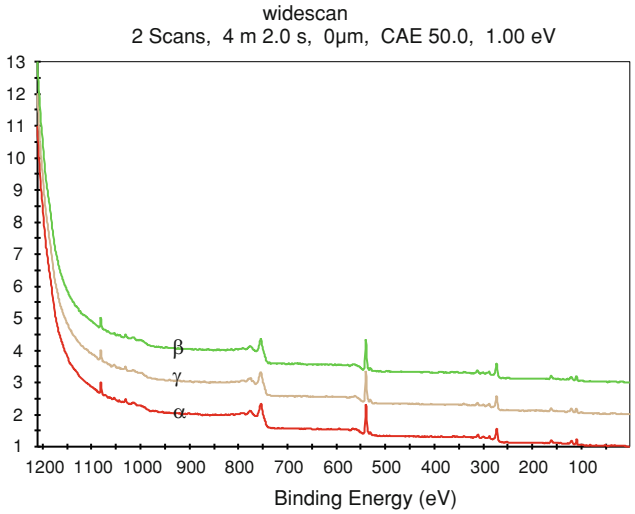

Fig. 5 Widescan XPS spectra of: native glass surface (α), glass surface after 3 etch runs using the ion gun (γ), and after femtosecond laser ablation (β)

In the case of the glass wafer ICP-etched in fluorine plasma, the composition of the surface changed due to formation of fluorine-, fluorosulphur-based, and fluorocarbon-based compounds. Numerous peaks can be observed in the XPS spectra of Fig. 6a, which correspond respectively (as a function of increasing electron binding energy) to peaks of sulfur (S2s, 225 eV), carbon (C1s, 285 eV), oxygen (O1s, 531 eV) and fluorine (F1s, 688.5 eV)

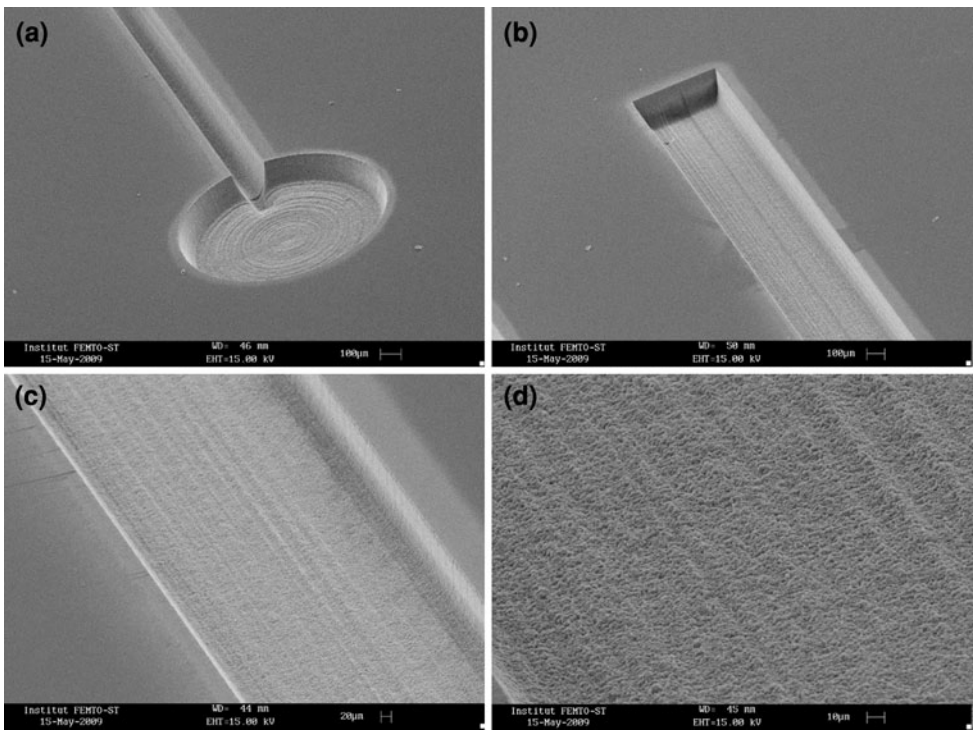

Fig. 4 SEM images of details of 100 µm wide and 140 µm deep microchannels with reservoir ablated in borosilicate glass: **a** channel with reservoir; **b** channel; **c** close-up of the channel; **d** close-up of the bottom of the channel showing the roughness (Ra 100–150 nm)

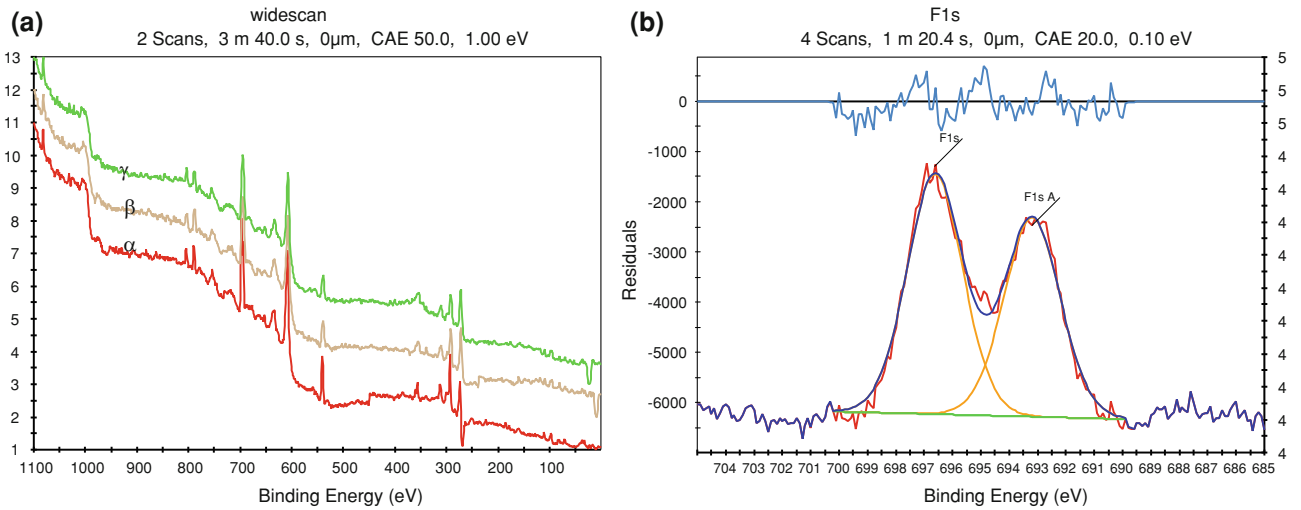

Fig. 6 **a** Widescan of glass surface ICP-etched in fluorine plasma with three levels of etch in XPS vacuum chamber (α to γ); **b** fluorine F1s spectra of glass surface after ICP etching

species. The intensity of the fluorine peaks is high, indicating a high proportion of fluorine species on the surface. The three levels of etching using the ion gun of the XPS analyzer did not change the intensity of the peaks, which means that the composition and chemical state of the surface do not change during etching. This type of XPS spectrum is characteristic of a fluorine plasma etched surface with a Teflon-like coating on the whole surface. Fluorine atoms are present at the surface in different molecular species, SF_3*, SF_4*, SF_5+, SF_6 and carbofluorine molecular species from C_4F_8. The second XPS graphic (Fig. 6b) shows two fluorine bond states likely representing F–S bond and F–C bond. We can only observe a little change in the carbon (C1s peak at 285 eV) intensity after three etch levels, which indicates that the etch removes the atmospheric contamination.

It is important to note that the fluorine compounds could alter the glass bonding process when bonding is performed at elevated temperature as they might desorb. It is the reason why we deposited an intermediate conductive thin film in order to decrease the temperature and the voltage of bonding.

3.5 Bonding

Anodic, a.k.a. electrostatic or field-assisted bonding, is a welding method using the effect of temperature and voltage. It is a robust process providing hermetic seals at relatively low temperature (<500°C) as compared with conventional sealing methods. Anodic bonding is widely used for bonding metals and non metals as well as integration and packaging of microsystems, in particular bonding silicon to glass, typically a structured silicon wafer (on the anode side) to an alkali-rich conductive borosilicate glass cover plate (on the cathode side) (Kanda et al. 1990). Anodic bonding of glass to glass was also demonstrated. The mechanism of glass-to-glass bonding is similar to a conventional silicon-to-glass electrostatic bonding. Such bonding can only be achieved using interlayers (Ju et al. 1998), and at least one intermediate layer such as amorphous silicon (Lee et al. 2000; Wei et al. 2004; Kutchoukov et al. 2004, Berthold et al. 2000, Lee et al. 2001), polysilicon (Berthold et al. 2000; Xue and Qiu 2005), silicon nitride, carbide or oxide or a combination of them (Berthold et al. 2000), or a titanium thin film interlayer (Briand et al. 2004; Mrozek 2009). With low temperature bonding, no appreciable flow of the glass occurs, hence enabling sealing around previously machined grooves, cavities, etc. without loss of dimensional tolerances. One of the challenges is to obtain a good and transparent bond at the end of the process as was demonstrated by Kutchoukov et al. (2004), and Mrozek (2009).

The process that was developed here involves depositing an intermediate conductive Si/Al/Si multilayer (20/40/20 nm) on the cover wafer of borofloat 33 glass. The silicon and aluminum layers were deposited respectively by 3-in. RF diode sputtering and 4-in. RF diode magnetron sputtering inside an Alcatel machine in the same run, without breaking the vacuum but only by changing the position of the substrate holder. The glass wafer was introduced in the vacuum chamber and first pumped with a primary rotative oil pump and a secondary turbo molecular pump down to 8×10^{-6} mbar. One-first step of etching was realized on the glass wafer with an RF power of 50 W, a pressure of 7×10^{-3} mbar in order to clean and degas the surface before starting the deposition run. Both 20 nm thick silicon layers were RF diode sputtered at a pressure of 1.2×10^{-2} mbar and a power of 400 W and the 40 nm

thick Al layer was RF magnetron diode sputtered at a pressure of 7×10^{-3} mbar with the same power. The polysilicon layer was obtained by sputtering a p-doped 3″ wafer of silicon and the aluminum from a 4″ pure 99.99% Al target. The targets were also pre-sputtered on a metallic shutter using the sputtering conditions at the beginning the process before deposition of the layers.

The coated glass cover wafer was anodically bonded to a second virgin glass wafer. This full wafer anodic bonding process was operated at 350°C with 1,500 V and under a load of 1,000 N, corresponding to a pressure of 0.227 MPa (2.27 bars), applied across the stack for 1 h under vacuum using an EVG 501 bonder. The multilayer coating when annealed at 350°C under vacuum changes its optical properties and becomes optically transparent, conferring to the bonded stack its optical transparency.

This anodic bonding process was also applied to seal a glass wafer microstructured by either micromachining technique described previously. Both wafers underwent a standard sulfochromic cleaning process at room temperature before bonding. In the case of the plasma etched wafer, the electroplated Ni mask was removed by a wet etch before the cleaning process.

Figure 7 shows microfluidic devices micromachined by plasma etching and femtosecond laser ablation and sealed by anodic bonding. For the plasma etched wafer, non uniformities in colour visible in the bonded stack (Fig. 7a) are due to height non-uniformity across the glass wafer due to over-etching of the Ni mask, but the area of the microfluidic circuit has bonded very well. For the laser ablated wafer, the uniformity and bonding across the wafer is fully satisfactory as can be seen in Fig. 7b.

The layer of aluminum was used in order increase the conductivity of the interlayer. The conductivity of a single silicon layer as used in the process developed by Kutchoukov et al. (2004) was not sufficient and required a high bonding temperature for a long time**.** Indeed Kutchoukov et al. (2004) used a chemically vapor deposited (LPCVD) 33 nm thick amorphous silicon layer and the bonding took place at 400°C for 1 h at 1,000 V after a preheating step of 2 h. Mrozek 2009 used an evaporated 40 or 80 nm thick titanium layer and obtained a fully transparent stack bonded at a temperature from 420 to 540°C in 0.5–5 min at 50–200 V after a pre-heating step of 20 min.

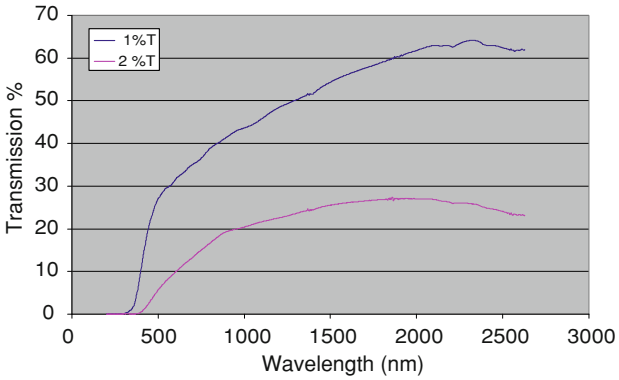

Fig. 8 Transmission of the bonded wafer assembly with the ICP-etched wafer as a function of the wavelength (curve 1: at the edge; curve 2: at the center of the wafer)

The process reported here compares favorably with those of the literature. The use of the multilayer system Al/Si/Al enabled a reduction in the temperature as well as bonding time of the process. In the case of ICP etched surface, this limited the diffusion of fluorine species which were fixed on the etched surface of the microstructures.

In Fig. 8 are reported the transmission curves in the visible spectrum of the bonded wafer assembly with the DRIE etched Borofloat 33 wafer, respectively at the edge (higher curve) and at the center (lower curve). We can see clearly that the edge is more transparent than the centre as the sputtered Si intermediate layer is not perfectly homogeneous in thickness as it was deposited using a 3″ target instead of a 4″ wafer, which leads to an homogeneity of ±17% on a 4″ wafer, that is a Si thickness of 100 nm in the centre and 66 nm at the edge of the 4″ wafer. Another point to be noted is the wavelength shift of the band pass towards smaller wavelengths at the edge of the wafer. This is probably due to a higher oxidation of the intermediate layer at the edge of the wafer during the anodic bonding step,

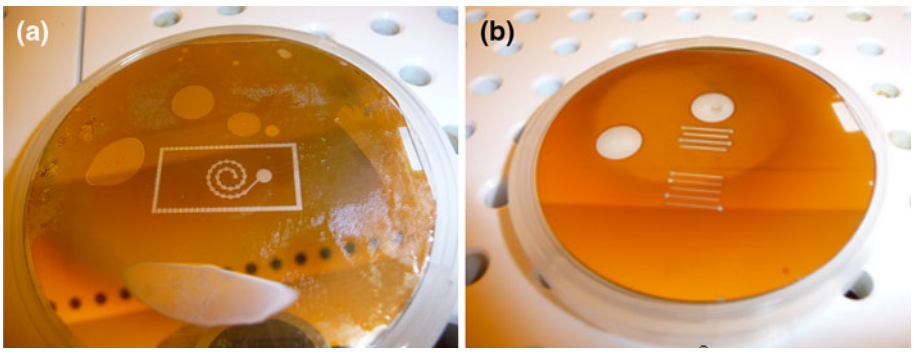

Fig. 7 **a** Optical images of microfluidic devices anodically bonded using an Si/Al/Si intermediate conductive layer: **a** bottom wafer of Borofloat 33 etched b y ICP-RIE; **b** bottom wafer of Pyrex® 7740 machined by femtosecond laser ablation

as the thickness difference cannot explain alone the large difference in transmission between the edge and the centre of the bonded wafer assembly.

4 Conclusion and outlook

Deep etching with nearly vertical walls was successfully demonstrated in borosilicate glass using ICP RIE in a fluorine plasma and a nickel electroplated mask. Deep etching of over 100 μm with a good anisotropy (83°–88°) and a low surface bottom roughness was achieved with a relatively good etching rate (on the order of 1 μm/mn) in a C_4F_8/O_2 plasma using an electrodeposited Ni mask. Those results are very competitive with those found in the literature.

ICP RIE etching of glass has the advantage of being a collective process which allows etching multiple microfluidic circuits with deep and almost vertical structures and high aspect ratio at the same time with good uniformity over the wafer. It is also attractive because the process can be extended from meso and micro-scale to nanometer-scale structure fabrication. Challenges still to be overcome include increasing the etching speed for deep microstructures with high aspect ratio as for example a hole of 100 μm will take over 1 h and half of etching time. Another challenge is to be able to develop simpler and faster processes for building a thinner and more resistant etching mask.

Femtosecond laser pulse ablation is a direct fabrication technique very well adapted to fast and precise prototyping of microfluidic devices in glass where the total volume of ablated material is rather small. Microfluidic circuits in borosilicate glass of 140 μm depth with good verticality (80–85°), edge sharpness and surface quality were successfully obtained. The bottom roughness is however higher than ICP RIE.

A challenge is to increase the aspect ratio which is presently on the order of 4–5. Modification of the optical path to reduce the laser beam size and change appropriately the beam shape (e.g. to obtain a square beam) would enable increasing the depth of the structures while maintaining vertical sidewalls, therefore increasing the aspect ratio.

Finally a process using anodic bonding was developed to produce a transparent seal between the micromachined glass wafers and a borosilicate glass cover wafer coated with a conductive interlayer.

Acknowledgments This work was carried out within the framework of the European Union (EU) Network of Excellence "Multi-Material Micro Manufacture: Technology and Applications (4M)" (EC funding FP6-500274-1; http://www.4m-net.org). We would like also to thank the Novalase Company for their support, and Dr. François Courvoisier, FEMTO-ST, for helpful discussions concerning the physical mechanisms associated with femtosecond lasers.

References

Akashi T, Yoshimura Y (2006) Deep reactive ion etching of borosilicate glass using an anodically bonded silicon wafer as etching mask. J Micromech Microeng 16:1051–1056

An R, Li Y, Dou Y, Liu D, Yang H, Gong Q (2006) Water-assisted drilling of microfluidic chambers inside silica glass with femtosecond laser pulses. Appl Phys A 83:27–29

An R, Uram JD, Yusko EC, Ke K, Mayer M, Hunt AJ (2008) Ultrafast laser fabrication of submicrometer pores in borosilicate glass. Opt Lett 33(10):1153–1155

Baram A, Naftali M (2006) Dry etching of deep cavities in Pyrex for MEMS applications using standard lithography. J Micromech Microeng 16:2287–2291

Bellouard Y, Said A, Dugan M, Bado P (2004) Fabrication of high-aspect ratio, micro-fluidic channels and tunnels using femtosecond laser pulses and chemical etching. Opt Express 12(10):2120–2129

Berthold A, Nicola L, Sarro PM, Vellekoop MJ (2000) Glass-to-glass anodic bonding with standard IC technology thin film as intermediate layers. Sens Actuator A 82:224–228

Briand D, Weber P, de Rooij NF (2004) Bonding properties of metals anodically bonded to glass. Sens Actuators A 114:543–549

Ceriotti L, Weible K, de Rooij NF, Verpoorte E (2003) Rectangular channels for lab-on-chip applications. Microelectronics Eng 67–68:865–871

Cheng Y, Sugioka K, Midorikawa K (2004) Microfluidic laser embedded in glass by three-dimensional femtosecond laser microprocessing. Opt Lett 29(17):2007–2009

Giridhar MS, Seong K, Schülzgen A, Khulbe P, Peyghambarian N, Mansuripur M (2004) Femtosecond pulsed laser micromachining of glass substrates with application to microfluidic devices. Appl Opt 43(23):4584–4589

Goyal A, Hood V, Tadigadapa S (2006) High speed anisotropic etching of Pyrex for microsystems applications. J Non-Cryst Solids 352:657–663

Ichiki T, Sugiyama Y, Taura R, Koidesawa T, Horiike Y (2003) Plasma applications for biochip technology. Thin Solid Films 435:62–68

Ju B-K, Choi W-B, Lee Y-H, Jung S-J, Lee N-Y, Han J-I, Cho K-I, Oh M-H (1998) Glass-to-glass electrostatic bonding for FED tubeless packaging application. Microelectronics J 29:839–844

Jung HC, Wang S, Hu X, Lee LJ, Lu W (2006) Etching of Pyrex glass substrates by ICP-RIE for micro/nanofluidic applications. J Vac Sci Technol B 24(6):3162–3164

Kanda Y, Matsuda K, Murayama C, Sugaya J (1990) The mechanism of field-assisted silicon-glass bonding. Sens Actuators A 23(1–3):939–943

Karnakis D, Knowles MRH, Alty KT, Schlar M, Snelling HV (2005) Comparison of glass processing using high repetition femtosecond (800 nm) and UV (255 nm) nanosecond pulsed lasers, Photonics West 2005, MOEMS-MEMS 22 January 2005

Kolari K (2008a) Deep plasma etching of glass with a silicon shadow mask. Sens Actuators A 141:677–684

Kolari K (2008b) Plasma etching of high aspect ratio structures on glass. In: Proceedings of 19th micromechanics Europe workshop, 28–30 September 2008, Aachen, Germany, pp 81–84

Kolari K, Saarela V, Franssila S (2008) Deep plasma etching of glass for fluidic devices with different mask materials. J Micromech Microeng 18:064010–064016

Kutchoukov VG, Laugere F, van der Vlist W, Pakula L, Garini Y, Bossche A (2004) Fabrication of nanofluidic devices using glass-to-glass anodic bonding. Sens Actuators A 114:521–527

Lee D-J, Ju B-K, Lee Y-H, Jang J, Oh M-H (2000) Glass-to-glass anodic bonding for high vacuum packaging of microelectronics and its stability. In: Proceedings of micro electro mechanical systems, 2000 (MEMS 2000) The thirteenth annual international conference, Issue 23–27:253–258

Lee D-J, Lee Y-H, Jang J, Ju B-K (2001) Glass-to-glass electrostatic bonding with intermediate amorphous silicon film for vacuum packaging of microelectronics and its applications. Sens Actuators 89:43–48

Li X, Abe T, Esashi M (2001) Deep reactive ion etching of Pyrex glass using SF6 plasma. Sens Actuators A 87:139–145

Li X, Abe T, Esashi M (2002) Fabrication of high-density electrical feed-throughs by deep-reactive-ion-ion etching of Pyrex glass. J Microelectromech Syst 11(6):625–630

Marcinkevičius A, Juodkazis S, Watanabe M, Miwa M, Matsuo S, Misawa H, Nishii J (2001) Femtosecond laser-assisted three-dimensional microfabrication in silica. Opt Lett 26:277–279

Maselli V, Osellame R, Martinez Vasquez R, Laporta P, Cerullo G (2007) Integration of optical waveguides and microfluidic channels fabricated by femtosecond laser irradiation, conference on lasers and electro-optics (CLEO) 2007 paper: CThS2, OSA Technical Digest Series (CD)

Mrozek P (2009) Anodic bonding of glasses with interlayers for fully transparent device applications. Sens Actuators A 151:77–80

Nikumb S, Chen Q, Li C, Reshef H, Zheng HY, Qiu H, Low D (2005) Precision glass machining, drilling and profile cutting by short pulse lasers. Thin Solid Films 477:216–221

Park JH, Lee N-E, Lee J, Park JS, Park HD (2005) Deep dry etching of borosilicate glass using SF_6 and SF6/Ar inductively coupled plasma. Microelectronic Eng 82:119–128

Queste S, Ulliac G, Jeannot J-C, Khan Malek C (2008) DRIE of non-conventional materials: first results. In: Dimov S, Menz W (eds) Proceedings of the 4th international conference on multi-material micro manufacture, 9–11 September 2008, Cardiff, pp 171–174

Sato T, Gumpenberger T, Kurosaki R, Kawaguchi Y, Narazaki A, Niino H (2007) Microfluidic bead array device using laser-machined surface microstructures on silica glass, conference on lasers and electro-optics (CLEO) 2007 paper: CThCC1, OSA Technical Digest Series (CD)

Schafer DN, Gibson EA, Salim EA, Palmer AE, Jimenez R, Squier J (2009) An optically integrated microfluidic cell counter fabricated by femtosecond laser ablation and anodic bonding, conference on lasers and electro-optics (CLEO) 2009 paper: CMMM1, OSA Technical Digest (CD)

Shah L, Tawney J, Richardson M, Richardson K (2001) Femtosecond laser deep hole drilling of silicate glasses in air. Appl Surf Sci 183:151–164

Thiénot E, Domingo F, Cambril E, Gosse C (2006) Reactive ion etching of glass for biochip applications: composition effects and surface damage. Microelectronic Eng 83:1155–1158

Wei J, Nai SML, Wong CK, Lee LC (2004) Glass-to-glass anodic bonding process and electrostatic force. Thin Solid Films 462–463:487–491

Xue Z, Qiu H (2005) Integrating micromachined fast response temperature sensor array in a glass microchannel. Sens Actuators 122:189–195